Journal of Civil Engineering and Architecture 19 (2025) 572-582
doi: 10.17265/1934-7359/2025.12.002

Reduction of Wind Loads on Ventilated Exterior Wall System Due to Gaps Provided in the Outer Wall

Yasushi Uematsu[1] and Keijiro Hosokawa[2]

1. New Industry Creation Hatchery Center, Tohoku University, Sendai 980-8579, Japan

2. NTT Urban Development, Tokyo 101-0021, Japan

Abstract: This paper investigates wind load reduction of ventilated exterior wall system, which has a ventilation layer behind the outer wall, by installing equally spaced horizontal gaps in the outer wall. The wind force on the outer wall is provided by the difference between the external pressure and the pressure in the ventilation layer (layer pressure). The gaps reduce the net wind forces on the outer wall due to pressure equalization. External pressures are obtained from a wind tunnel experiment using a scale model of the building, while the layer pressures are obtained from a numerical simulation using the unsteady Bernoulli equation applied to the gap flows and the cavity flows in the ventilation layer. The effects of gap width g and gap spacing s on the layer pressures are examined. The results indicate that the larger the gap width and/or the smaller the gap spacing, the greater the reduction in wind forces on the outer wall. However, the layer pressures, which act on the interior wall as external pressures, increase in magnitude. Discussion is made of the optimal combination of g and s, which effectively reduces the wind forces on the outer wall without increasing the magnitude of layer pressures as much.

Key words: Ventilated exterior wall system, wind load, gap, wind tunnel experiment, numerical simulation, unsteady Bernoulli equation, pressure equalization.

1. Introduction

Recently, ventilated exterior wall systems using metal or ceramic siding, which have ventilation layers behind the siding (see Fig. 1), are often used for low-rise residential houses in Japan. Many studies have been conducted on the environmental aspects of this wall system such as temperature, condensation and mold (e.g., Rahiminejad et al. [1] and Li et al. [2]). By comparison, little research has been done on the structural aspects such as wind loads and wind resistance.

For discussing the wind resistance of ventilated exterior wall systems, it is necessary to estimate the pressures in the ventilation layer (called "layer pressures" in this paper), because the net wind force on the outer wall (siding) is provided by the difference between the external pressure and the layer pressure. Wind loads on double skin curtain wall systems, which are similar in shape to ventilated exterior wall systems, have been investigated by many researchers (e.g., Xu et al. [3]). However, the results of those studies cannot be applied to the ventilated exterior wall systems, because the layer thickness of ventilated exterior wall systems is much smaller than that of double skin curtain wall systems. Furthermore, the boundary conditions of these systems are different from each other.

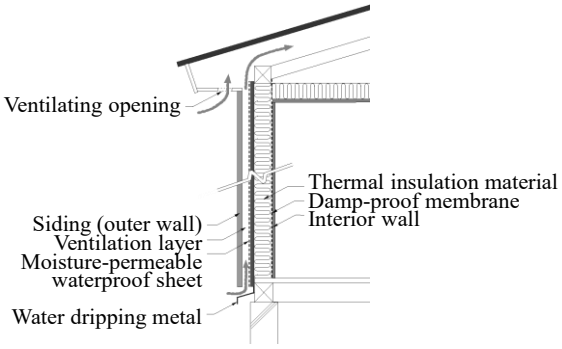

Fig. 1 An example of ventilated exterior wall system.

Corresponding author: Yasushi Uematsu, Dr. Eng., senior research fellow, research fields: wind engineering, snow engineering and steel structure.

Wind pressures on the external surface of the outer wall (siding) can be obtained from a wind tunnel experiment using a scale model of the building. However, it is difficult to measure the layer pressures in the wind tunnel experiment, because the ventilation layer is too thin to be reproduced in the wind tunnel model. Thus, Watanabe and Uematsu [4] proposed a numerical simulation for estimating the layer pressures, in which they applied the unsteady Bernoulli equation to the flows through the gaps (gap flows) and the flows in the ventilation layers (cavity flows). They used the time histories of external wind pressure coefficients at the location of gaps in the outer walls as the boundary conditions, which were obtained from a wind tunnel experiment. They considered very small gaps at the joints of metal siding as well as the openings at the top and bottom of the ventilated exterior wall system. The results indicated that the net wind forces on the outer wall were reduced significantly because of pressure equalization. Then, if gaps are intentionally made in the middle of the outer wall, the pressure equalization may be more promoted, generating further reduction of wind forces on the outer wall.

This paper investigates the effects of equally spaced horizontal gaps on the wind load reduction of ventilated exterior wall systems using the same method that Watanabe and Uematsu [4] developed. The gaps may increase the magnitude of layer pressures. Since the layer pressures act on the outer surface of the interior wall as external pressures, we focus on the optimal combination of gap width g and gap spacing s which effectively reduces the net wind forces on the outer wall without increasing the magnitude of layer pressures as much. Note that the interior walls are generally weaker against inward forces than outward forces.

2. Investigated Building

The investigated building is a low-rise residential house having a gable roof with 22° pitch and 0.6 m overhang (see Fig. 2). The width and depth are both 10 m. The eaves height is 6 m. The exterior walls are constructed of horizontal metal siding 15 mm thick and 400 mm wide. The spacing between vertical furring strips 45 mm wide and 18 mm thick, which are supported by studs behind them, is 455 mm. Thus, the ventilation layer is 410 mm wide and 18 mm deep. The opening widths of the wall system at the top and bottom are 18 mm and 10 mm, respectively. The opening at the top is open to the outside (expressed as "EX", Fig. 3a) or to the attic (expressed as "AT"). In the latter case, the pressure at the top opening is equal to that of the attic, which depends on the location and area of ventilation openings in the attic. We consider three types of attic ventilation methods, as shown in Fig. 3. "AT-e" has ventilation openings in the eaves (Fig. 3b). "AT-g" has ventilation openings near the top of the gable walls (Fig. 3c). "AT-eg" has ventilation openings both in the eaves and near the top of the gable walls

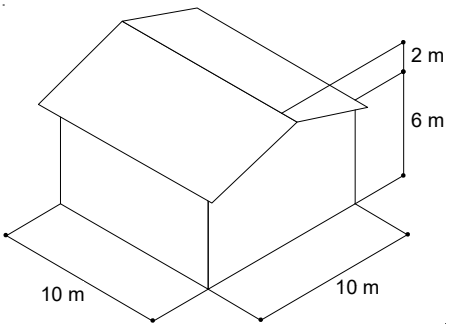

Fig. 2 Investigated building.

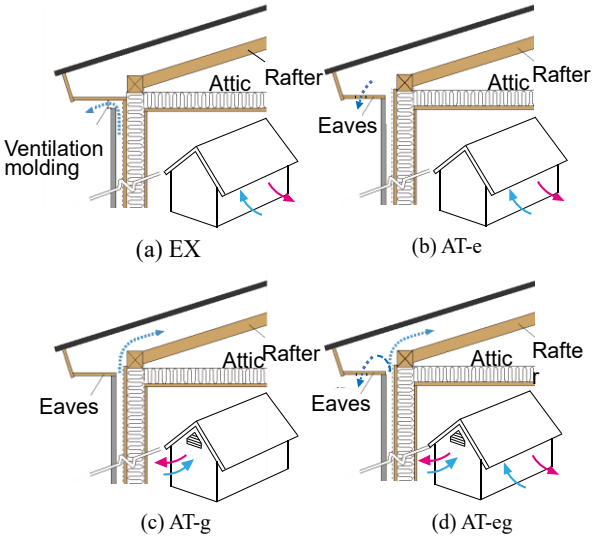

Fig. 3 Schematic illustrations of the opening conditions at the top of the wall system.

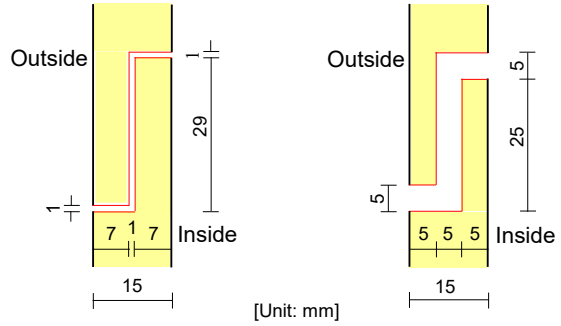

(a) g = 1 mm (b) g = 5 mm

Fig. 4 Gaps intentionally provided in the middle of the outer wall (cross section).

(Fig. 3d). The configuration of the equally spaced horizontal gaps intentionally provided in the middle of the outer wall is set as shown in Fig. 4, considering the waterproofing. The gap width g is either 1 mm or 5 mm, and the gap spacing s between gaps is changed from 0.8 m to 2.0 m at a step of 0.4 m.

3. Wind Tunnel Experiment for Measuring External Pressures on the Walls

3.1 Experimental Model and Procedure

The wind tunnel model is made of acrylic plates at a geometric scale of 1/100 (Fig. 5). A total of 72 and 60 pressure taps of 0.6 mm internal diameter are installed almost uniformly on a gable wall and a side wall, respectively. The wind tunnel flow is a turbulent boundary layer. The power law exponent for the mean wind speed profile is about 0.21. The intensity and integral scale of turbulence at the mean roof height H are about 0.16 and 0.2 m, respectively. The wind direction θ, defined as shown in Fig. 5, is changed from 0° to 180° for the gable wall and from -90° to 90° for the side wall at an increment of 10°, considering the symmetry of the model. The mean wind speed U_H at the mean roof height H is set at 9 m/s. Assuming that the design wind speed is U_H = 27.8 m/s, the velocity scale of the wind tunnel flow is 1/3.1, resulting in the time scale of 1/32.4. The Reynolds number Re, defined by $Re = U_H H/\nu$, with ν being the kinematic viscosity of air, is about 4.2×10^4. The blockage ratio Br, defined as the ratio of the model's vertical cross-sectional area to that of the wind tunnel, is about 0.71% at most. The values of Re and Br satisfy the requirements of the ASCE Wind Tunnel Testing for Buildings and Other Structures [5], that is, $Br < 5\%$ and $Re > 1.1 \times 10^4$.

The pressure taps are connected to a multi-channel differential pressure transducer (Wind Engineering Institute, MAPS-02) via flexible vinyl tubes of 1 mm inside diameter and 1 m length. The wind pressures at all pressure taps on the side or gable wall are sampled simultaneously at a sampling frequency of 800 Hz during a sampling time of 18.5 s which corresponds to 10 min at full scale. Low-pass filters with a cut-off frequency of 300 Hz are used to remove high-frequency electrical noise. The distortion of the measured pressures due to the tubing and the low-pass filter is compensated by using the frequency response function of the measuring system in the frequency domain (Irwin et al. [6]). The measurements are repeated 10 times under the same condition. The wind pressures are normalized by the velocity pressure q_H ($= \frac{1}{2}\rho U_H^2$, with ρ being air density) at the mean roof height H to yield the external wind pressure coefficients C_{pe}. The statistical values of wind pressure coefficients and others are evaluated by applying ensemble averaging to the results of 10 consecutive runs.

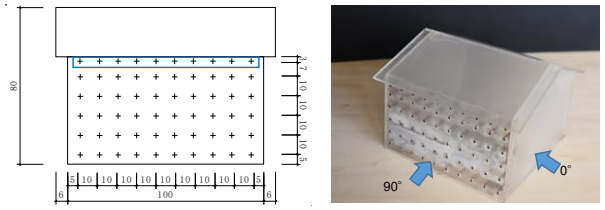

(a) Side wall

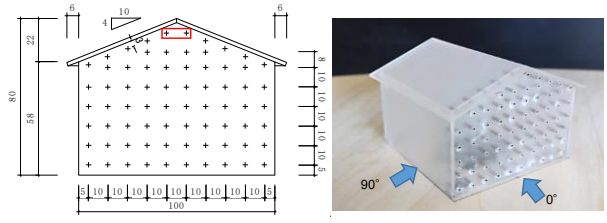

(b) Gable wall

Fig. 5 Wind tunnel model and pressure tap arrangement.

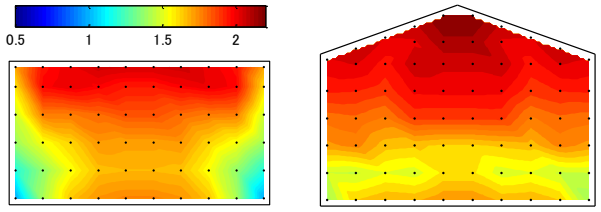

(a) Maximum peak wind pressure coefficient

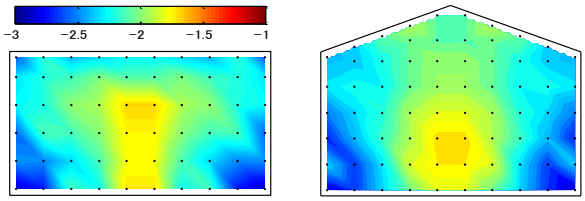

(b) Minimum peak wind pressure coefficient

Fig. 6 Distributions of $\hat{C}_{pe,\mathrm{cr}}$ and $\check{C}_{pe,\mathrm{cr}}$ on the side and gable walls.

3.2 Experimental Results

Fig. 6 shows the distributions of the most critical maximum and minimum peak wind pressure coefficients, $\hat{C}_{pe,\mathrm{cr}}$ and $\check{C}_{pe,\mathrm{cr}}$, irrespective of wind direction on the side and gable walls, respectively. The values of $\hat{C}_{pe,\mathrm{cr}}$ are large at the top center of the wall when the wind direction is nearly normal to the wall. On the other hand, the magnitude of $\check{C}_{pe,\mathrm{cr}}$ is large at the lower level of the windward edge of the wall when the wind direction is inclined 10° to 20° to the wall. This feature may be related to the generation of a conical vortex with an apex at the base of the building [7]. It is thought that peak wind forces on the outer wall become large under such a condition.

4. Numerical Simulation of Layer Pressures

4.1 Outline of the Simulation Method

The method employed in this study is the same as that Watanabe and Uematsu [4] developed. Here, only the overview of the method is described.

Assuming that there is no gap between the inside surface of the outer wall and the furring strip, we consider the vertical flow in the ventilation layer from the bottom opening to the top opening. The bottom opening is assumed to be located at a height of 500 mm from the ground. The width L_H and depth d of the ventilation layer are 410 mm and 18 mm, respectively. Not only the intentionally provided horizontal gaps (Fig. 4) but also small gaps at the joints of siding are considered. The ventilation layer is divided into virtual subspaces, as shown in Fig. 7, which are called "Rooms" in this paper. It is assumed that the pressure inside each room is kept constant. A volume of air flows in or out of each room through the gap and the boundaries between adjacent Rooms (see Fig. 7). Now, we focus on Room j. The driving force of the gap flow is the difference between the external pressure ${}_eP_j$ at the gap location and the layer pressure P_j. Applying the unsteady Bernoulli equation to the gap flow, the velocity ${}_eU_j$ of the gap flow may be given by the following equation of motion:

$$\rho l_e \, {}_e\dot{U}_j = P_j - {}_eP_j - \left(\frac{1}{k_e}\right)^{\frac{1}{n}} \left(\frac{\rho}{2}\right)^{\frac{1}{2n}} {}_eU_j \left|{}_eU_j\right|^{\frac{1}{n}-1} - \frac{64\nu}{{}_eU_j d_e} \frac{\rho l_e}{2d_e} \, {}_eU_j \left|{}_eU_j\right| \tag{1}$$

where superscript dot represents the derivative with respect to time t; l_e and d_e are the effective depth and width of the gap, respectively; k_e is the coefficient of discharge; and n represents a flow index that depends on the shape of gap (0.5–1.0). According to Oh et al. [8], l_e is approximated by the following equation:

$$l_e = l_0 + 0.89\sqrt{A_e} \tag{2}$$

where l_0 and A_e are the actual depth and area of the gap. ${}_eP_j$ is provided by the following equation using the external wind pressure coefficient C_{pej} at the gap location:

$${}_eP_j = \frac{1}{2}\rho U_H^2 \cdot C_{pej} \tag{3}$$

Similarly, the driving force of the cavity flow in the ventilation layer is the difference between layer pressures in adjacent Rooms. Thus, the equation of motion for the cavity flow past the boundary between Rooms j and j+1, the velocity of which is expressed

as ${}_jU_{j+1}$, may be provided by the following equation:

$$\rho L_V \, {}_j\dot{U}_{j+1} = P_j - P_{j+1} - C_{Lz}\frac{\rho}{2} \, {}_jU_{j+1}\left|\, {}_jU_{j+1}\right| - \frac{6\nu}{{}_jU_{j+1}L_H}\frac{\rho L_V}{2L_H} \, {}_jU_{j+1}\left|\, {}_jU_{j+1}\right| \quad (4)$$

where C_{Lz} is pressure loss coefficient (= $1/\sqrt{k_z}$, with k_z being the coefficient of discharge of the cavity flow; and L_H and L_V represent the width and length of the Room, respectively. The equation of motion for the cavity flow past the boundary between Rooms j-1 and j, the velocity of which is expressed as ${}_{j-1}U_j$, is provided by the same formula as Eq. (4).

Assuming the weak compressibility of the air and adiabatic condition, the pressure change in Room j may be expressed by the following equation based on the mass conservation law:

$$\dot{P}_j = \frac{\gamma P_0}{V_0}\sum_{m=1}^{N} k_m A_m U_m \quad (5)$$

where γ is the ratio of specific heat of air (= 1.4); k_m, A_m and U_m represent the coefficient of discharge, area and flow velocity at the m-th gap or boundary with the next Room; and N is the total number of gaps and boundaries existing in Room j.

The mass conservation law determines the pressure P_j in the Room, which is normalized by q_H and referred to as "layer pressure coefficient" C_{pl}. The wind force coefficient C_f on the outer wall is given by $C_{pe} - C_{pl}$. Note that C_{pl} corresponds to the external pressure coefficient on the interior wall, which is not considered in conventional design of ventilated exterior wall systems in Japan. Using Eqs. (1)-(4) together with the time histories of external wind pressure coefficients at the location of gaps, which were obtained from the above-mentioned wind tunnel experiment, we can calculate the velocities of the gap flow and the cavity flow past the boundaries with the next Rooms. Then, substituting them into Eq. (5), we can obtain simultaneous equations for the layer pressures in all Rooms. These equations can be solved numerically using the fourth-order Runge-Kutta method. The time step Δt is set to 1/8,000 s based on the results of Watanabe and Uematsu [4] who investigated the stability and accuracy of the solution. The sampling interval of the pressure measurements in the wind tunnel experiment is approximately 1/25 s (= 1/800 s × 32.4) at full scale, which is much longer than Δt. Therefore, the cubic spline function is applied to the time histories of wind pressure coefficients C_{pej} for interpolation. Furthermore, since the location of pressure taps on the wind tunnel model does not coincide with that of gaps, the cubic spline function is again applied to the wind tunnel data of C_{pe} to obtain the values at the location of gaps. Regarding the details of the simulation method, refer to Watanabe and Uematsu [4] and Uematsu et al. [9, 10].

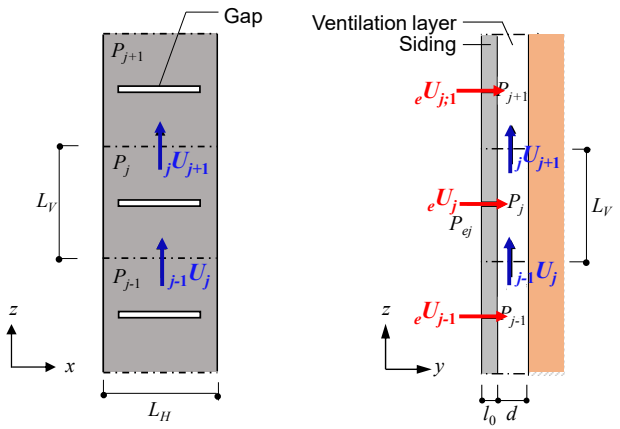

Fig. 7 Schematic illustration of the flows and pressures.

The characteristic values of the gap flow included in the above-mentioned equations, such as the coefficient of discharge, are determined based on the experiments using a full-scale model of the gap and a "time-varying wind PLA (pressure loading actuator)" developed by Gavanski et al. [11]. Fig. 8 shows a schematic illustration of the experimental setup for measuring the coefficient of discharge for the gap. A full-scale model of the gap is installed in the pressure chamber, and the pressure in the chamber is reduced step by step using the PLA. The pressure difference ΔP between the two sides of the gap and the flow rate Q through the gap are measured by a differential pressure transducer and a current meter, respectively. In general, the relation

between Q and ΔP is represented by the following equation:

$$Q = k_e A_e \left(\frac{2}{\rho}\Delta P\right)^n \quad (6)$$

where k_e = coefficient of discharge; and A_e = area of the gap. The value of $k_e A_e$ represents the equivalent area of the gap. Fig. 9 shows the experimental results for the $Q - \Delta P$ relation at g = 1 mm and 5 mm, respectively. The solid line in each sub-figure represents the relation provided by Eq. (6), which was obtained by applying the least squares method to the experimental results as n = 0.5. The value of k_e is 0.315 for g = 1 mm and 0.366 for g = 5 mm. Watanabe and Uematsu [4] conducted a detailed investigation of the gap flow at the joints of metal siding with complex geometries using the same method. They found that n is nearly equal to 0.65 and the value of $k_e A_e$ is one order of magnitude smaller than that of the gaps considered here (Fig. 4). This feature indicates that the effect of the gaps at the joints of siding on the layer pressures is much smaller than that of the intentionally provided gaps.

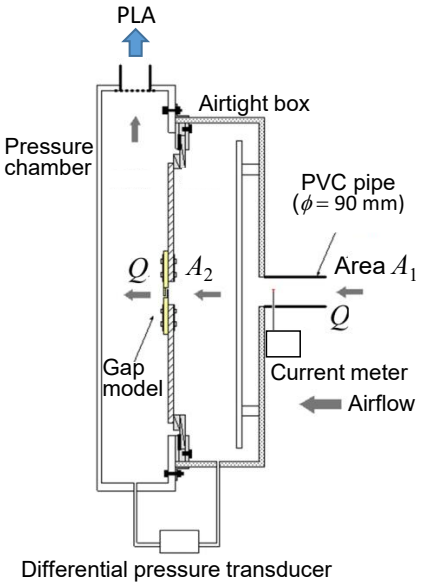

Fig. 8 Schematic illustration of the experiment for measuring the coefficient of discharge.

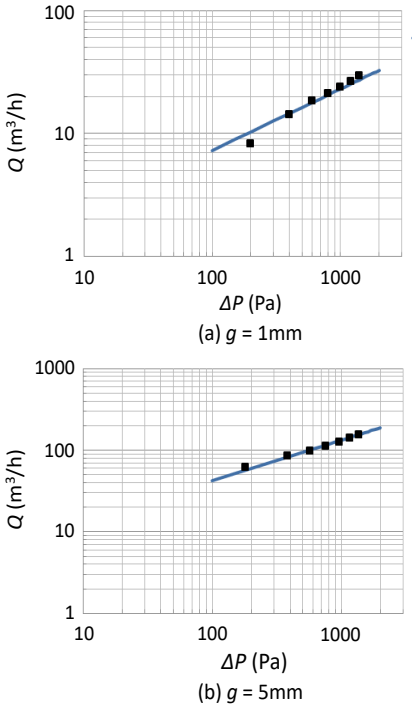

Fig. 9 Relation between Q and ΔP.

Watanabe and Uematsu [4] investigated the flows past the openings of ventilation layer at the top and bottom as well as the flow inside the ventilation layer based on an experiment using a four-room model and the numerical simulation. They obtained the values of coefficient of discharge for these flows are as follows; that is, $k_e \approx$ 0.36 and 0.30 for the flows past the top and bottom openings, respectively, and $k_e \approx$ 0.90 for the flow in the ventilation layer. Furthermore, we can assume that n = 1 for these flows.

4.2 Results and Discussion

This section focuses on the side wall. Fig. 10 shows the location of vertical furring strips, joints of horizontal siding and boundaries between Rooms. The location of pressure taps on the wind tunnel model is also shown in the figure. When the top of the wall system is open to the outside (EX), the pressure at the opening coincides with the external pressure at the opening. On the other hand, when the opening is open to the attic (AT), the pressure at the opening coincides with the attic pressure P_{attic}. The value of P_{attic} depends on the area and location of attic ventilation openings. Since the areas of attic ventilation openings are generally very small with respect to the attic volume,

the fluctuation of attic pressure is expected to be very small. Therefore, only the time-averaged attic pressure $\bar{P}_{\text{attic}}$ is considered here. The value of $\bar{P}_{\text{attic}}$ is provided by the weighted average of the mean external pressures at the location of the ventilation openings, weighted by the ventilation opening area. Since the area and location of attic ventilation openings vary from building to building in practice, it is difficult to generalize the value of $\bar{P}_{\text{attic}}$. Therefore, we assume that $\bar{P}_{\text{attic}}$ is given as follows for each of the three cases of attic ventilation openings, AT-e, AT-g and AT-eg (see Fig. 3):

AT-e: Average of the external pressures at pressure taps just below the eaves of the side walls (taps in a rectangle in Figure 5a; 20 taps on both sides);

AT-g: Average of the external pressure at two pressure taps near the apex of gable wall (taps in a rectangle in Figure 5b; 4 taps on both sides);

AT-eg: Average of external pressures at a total of 24 taps considered in the cases of AT-e and AT-g.

$\bar{P}_{\text{attic}}$ is normalized by q_H and expressed as $\bar{C}_{p,\text{attic}}$. Fig. 11 shows the variation of $\bar{C}_{p,\text{attic}}$ with wind direction θ. Corresponding to the change in the distribution of mean external wind pressure coefficients on the walls, the value of $\bar{C}_{p,\text{attic}}$ changes with θ significantly. As might be expected, the results for "AT-e" and "AT-g" show opposite trends. When the wind direction is normal to a gable wall, i.e., at θ = 0° or 180°, $\bar{C}_{p,\text{attic}}$ is positive for "AT-g" but negative for "AT-e". On the other hand, when the wind direction is normal to a side wall, i.e., at θ = 90° or -90°, $\bar{C}_{p,\text{attic}}$ is positive for "AT-e" but negative for "AT-g". In the case of "AT-eg", $\bar{C}_{p,\text{attic}}$ is generally negative, ranging from -0.2 to -0.4.

Fig. 12 shows the distributions of the maximum peak layer pressure coefficients $\hat{C}_{pl}$ at θ = 80°, where positive external pressure coefficients on the side wall are large, for three cases of gap condition. Similarly, Fig. 13 shows the distributions of the minimum peak layer pressure coefficients $\check{C}_{pl}$ at θ = 20°, where negative external pressure coefficients on the side wall are large in magnitude. In the no-gap case, the magnitude and the spatial variation of $\hat{C}_{pl}$ and $\check{C}_{pl}$ are both small. With gaps provided in the middle of the outer wall, both the magnitude and the spatial variation become large. These features of $\hat{C}_{pl}$ and $\check{C}_{pl}$ are related to the pressure equalization generated by the gaps. The pressure equalization causes a reduction in net wind forces on the outer wall. However, the gaps increase the magnitude of peak layer pressures at the

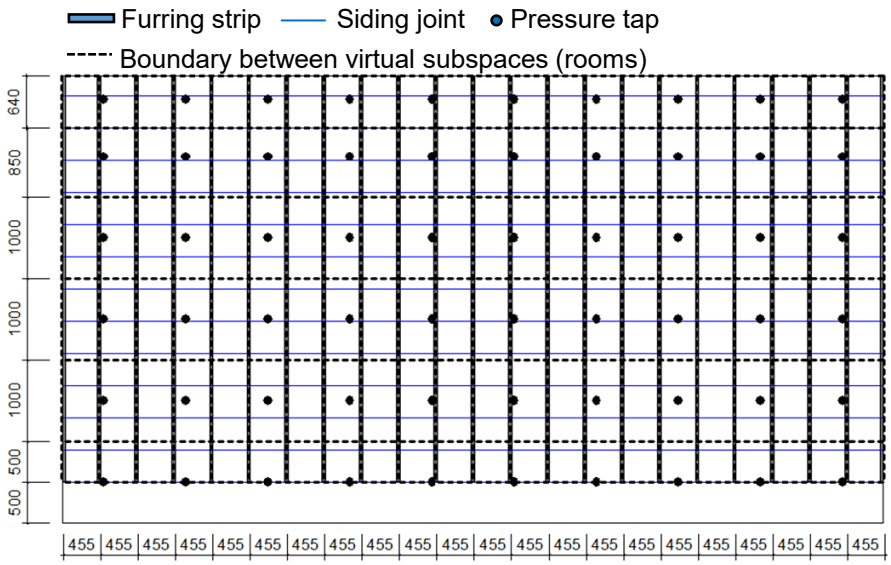

Fig. 10 Configuration of the side wall and location of pressure taps.

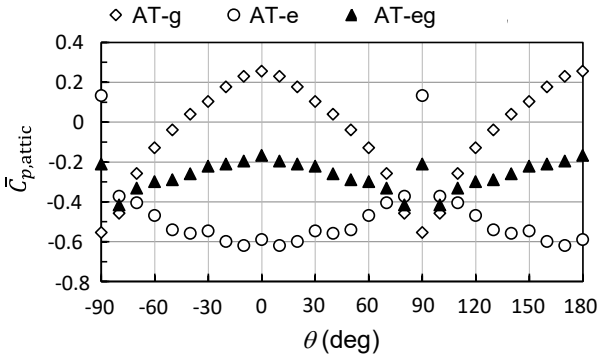

Fig. 11 Variation of $\bar{C}_{p,\mathrm{attic}}$ with wind direction θ.

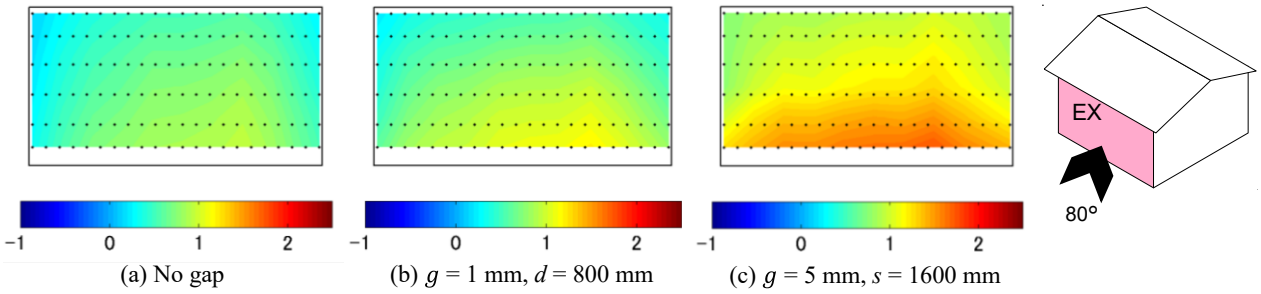

(a) No gap (b) g = 1 mm, d = 800 mm (c) g = 5 mm, s = 1600 mm

Fig. 12 Distributions of the maximum peak layer pressure coefficients $\hat{C}_{pl}$ at θ = 80°.

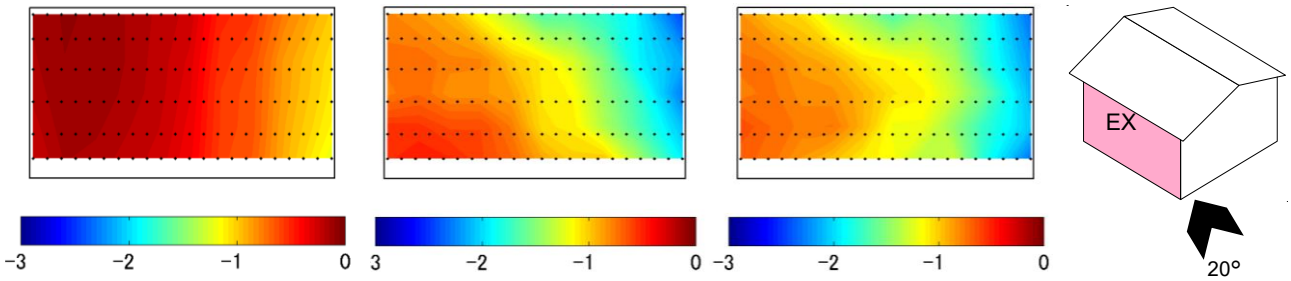

Fig. 13 Distributions of the minimum peak layer pressure coefficients $\check{C}_{pl}$ at θ = 20°.

same time. It should be noted that the layer pressures act on the interior walls as external pressures. The net wind force on the interior wall is provided by the difference between layer pressure and internal pressure of the building. In the Building Standard Law of Japan, the peak internal pressure coefficient for designing cladding/components of enclosed buildings with no predominant openings is specified as 0 or -0.5. The values of 0 and -0.5 may be combined with $\check{C}_{pl}$ and $\hat{C}_{pl}$, respectively, when estimating the design wind loads on the interior walls. Thus, the layer pressure plays an important role in the structural design of interior walls.

In practice, the construction method of ventilated exterior wall systems, such as the spacing between furring strips and the specification of screws for fastening siding to the furring strips, is not changed from place to place. It is generally determined based on the largest loads on the siding. Therefore, focus is on the maximum and minimum peak values of C_f and C_{pl} among all points on the wall. Figs. 14 and 15 respectively show the variation of the maximum and minimum peak values of C_f and C_{pl} with wind direction θ for the four attic ventilation methods when g = 1 mm and s = 800 mm. The subscripts "0" and "1" indicate the results for the no-gap and with-gap cases, respectively. The results for $\hat{C}_{pe}$ and $\check{C}_{pe}$ are also plotted in the figures. The values of $\hat{C}_f$ and $\hat{C}_{pe}$ are maximum at $\theta \approx 90°$, while the values of $\check{C}_f$ and

$\check{C}_{pe}$ are minimum (maximum in magnitude) at θ = 10°-20°. At these wind directions, the magnitudes of $\hat{C}_{pl}$ and $\check{C}_{pl}$ are much smaller than those of $\hat{C}_{pe}$ and $\check{C}_{pe}$, respectively. The values of $\hat{C}_{f1}$ and $\check{C}_{f1}$ (with gaps) are generally smaller in magnitude than $\hat{C}_{f0}$ and $\check{C}_{f0}$ (without gaps), respectively, indicating that the wind forces on the outer wall are significantly reduced by the gaps due to the effect of pressure equalization.

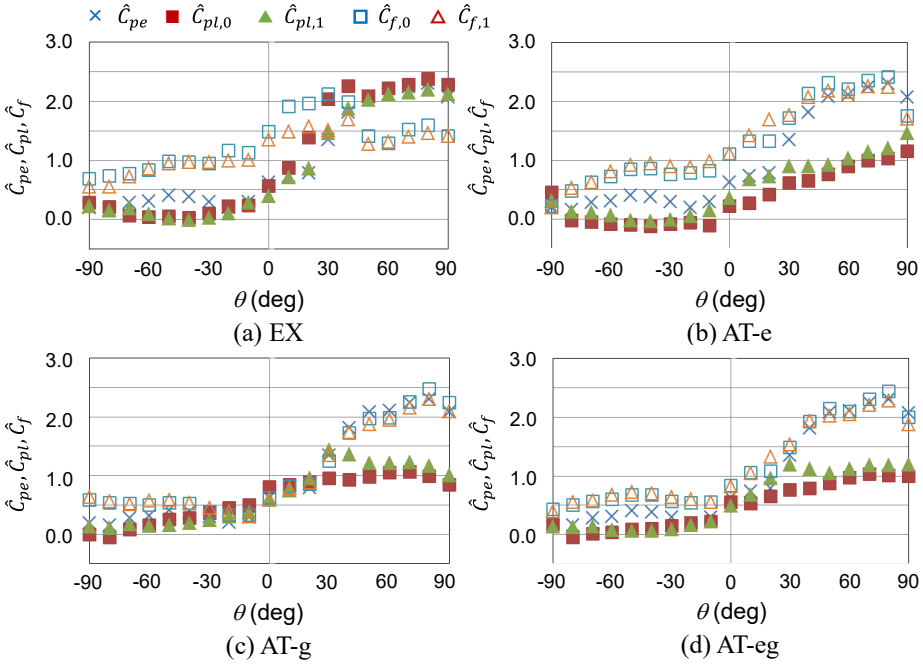

Fig. 14 Variation of the maximum wind force and wind pressure coefficients among all points with wind direction θ (g = 1 mm, s = 800 mm).

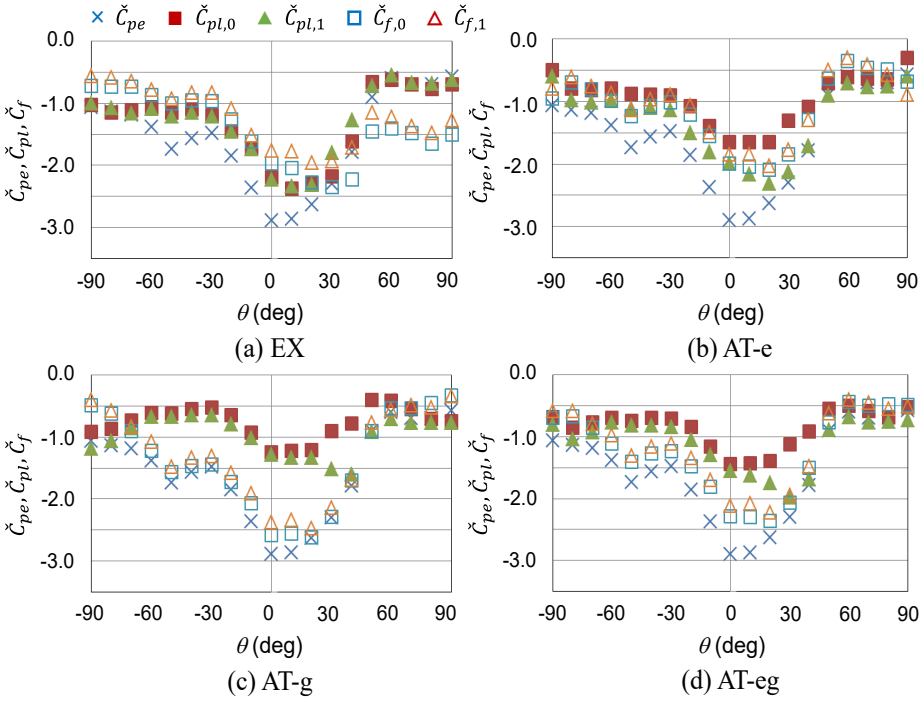

Fig. 15 Variation of the minimum wind force and wind pressure coefficients among all points with wind direction θ (g = 1 mm, s = 800 mm).

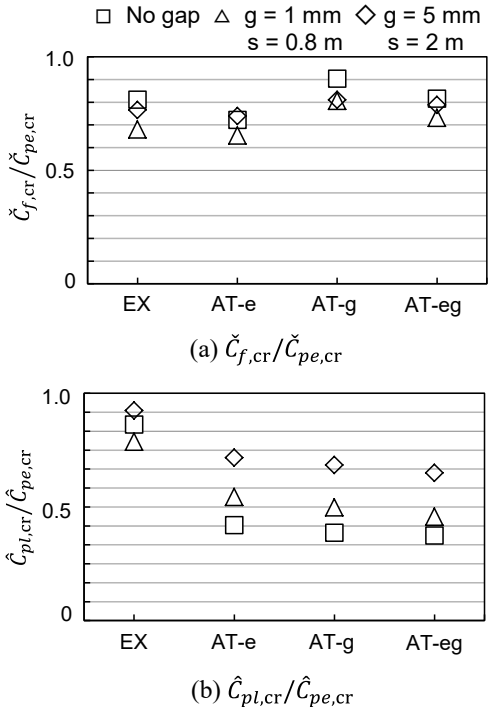

Fig. 16 $\check{C}_{f,\mathrm{cr}}/\check{C}_{pe,\mathrm{cr}}$ and $\hat{C}_{pl,\mathrm{cr}}/\hat{C}_{pe,\mathrm{cr}}$ ratios for different attic ventilation methods.

In usual construction methods, the siding is fastened to the furring strips with screws from the outside. Consequently, the strength of the siding is lower in the outward direction than in the inward direction. Therefore, $\check{C}_f$ is more important than $\hat{C}_f$ for the siding. The gaps reduce the magnitude of $\check{C}_f$ at θ = 10°-20°. However, the gaps increase $\hat{C}_{pl}$ at $\theta \approx 90°$. As mentioned above, the layer pressures act on the interior walls (plasterboards are usually used) as external pressures. Since the interior walls are usually fastened to studs with screws or nails from the inside, $\hat{C}_{pl}$ is more important than $\check{C}_{pl}$ for the interior walls. Thus, focus is on the most critical minimum peak wind force coefficient $\check{C}_{f,\mathrm{cr}}$, the most critical minimum peak external pressure coefficient $\check{C}_{pe,\mathrm{cr}}$, the most critical maximum peak layer pressure coefficient $\hat{C}_{pl,\mathrm{cr}}$ and the most critical maximum external pressure coefficient $\hat{C}_{pe,\mathrm{cr}}$ irrespective of wind direction. Note that the external pressure coincides with the net wind force on the outer wall when the layer pressure or the internal pressure is zero. Furthermore, the layer pressure coincides with the external pressure when the perfect pressure equalization is exerted. Figs. 16a and 16b show the $\check{C}_{f,\mathrm{cr}}/\check{C}_{pe,\mathrm{cr}}$ and $\hat{C}_{pl,\mathrm{cr}}/\hat{C}_{pe,\mathrm{cr}}$ ratios, respectively. The gap spacing s is set to 800 mm for g = 1 mm and 1,600 mm for g = 5 mm. The net wind forces on the outer wall are reduced by the gaps significantly. Furthermore, the wind pressures acting on the interior wall (layer pressures) are smaller in magnitude than the external pressures. The effects of gaps on the wind forces on the outer wall and the layer pressures depend on g and s significantly. In general, with an increase in g and/or a decrease in s, the net wind forces on outer walls decrease in magnitude, which is desirable for the outer wall. However, the layer pressures increase with gaps, which is not desirable for the interior walls. In the case of "EX", the value of $\hat{C}_{pl,\mathrm{cr}}$ is comparable to $\hat{C}_{pe,\mathrm{cr}}$. The combination of g and s that effectively reduces the net wind forces on the outer wall without increasing the magnitude of layer pressures as much is important when considering the wind resistance of the ventilated exterior wall systems. Within the limits of the present analysis, a combination of g = 1 mm and s = 800 mm seems to be optimal. In this case, the reduction in $|\check{C}_{f,\mathrm{cr}}|$ is significant and the value of $\hat{C}_{pl,\mathrm{cr}}$ is close to that for the no-gap case.

5. Concluding Remarks

We have proposed providing equally spaced horizontal gaps in the middle of the outer walls of ventilated exterior wall systems to improve the wind resistance. The wind force on the outer wall is provided by the difference between external pressure and layer pressure (pressure in the ventilation layer). The gaps could reduce the net wind forces on the outer walls significantly due to pressure equalization.

This paper investigated the effects of gap width g and gap spacing s on the wind loading of the ventilated exterior wall systems. The external wind pressures were obtained from a wind tunnel experiment using a scale model of the building. On the other hand,

the layer pressures were obtained from a numerical simulation using the unsteady Bernoulli equation applied to the flows though the gaps (gap flows) and the flows in the ventilation layers (cavity flows). The results indicate that the larger the gap width and/or the smaller the gap spacing, the greater the reduction in wind forces on the outer walls. However, the layer pressure conversely increases in magnitude with increasing g and/or decreasing s. Considering that the layer pressures act on the interior walls as external pressures, these results imply that the gaps are advantageous for the outer walls but disadvantageous for the interior walls. In practical design, the layer pressure is not considered even for usual ventilated exterior wall systems with no gaps. Watanabe and Uematsu [4] argued for the need to evaluate the wind resistance of the interior walls. Then, Hosokawa [12] investigated the load bearing capacity of interior walls made of plaster boards under uniform suction.

The present results may be useful for discussing the wind resistance of ventilated exterior wall systems. It is important to find the optimal combination of g and s that effectively reduces the net wind forces on the outer wall without increasing the magnitude of layer pressure as much, considering that the load bearing capacity of interior walls is lower than the outer walls. Within the limits of the present study, a combination of g = 1 mm and s = 800 mm seems to be optimal. Since the optimal combination may depend on the flow condition and building shape, more investigations are needed. This is the subject of our future study.

References

[1] Rahiminejad, M., Paris, A. L. M., Ge, H., and Khovalyg, D. 2022. “Performance of Lightweight and Heavyweight Building Walls with Naturally Ventilated Passive and Active Facades.” *Energy and Buildings* 256: 111751.

[2] Li, J., Cai, Q., Wang, X., Liu, F., Yu, H., Liu, J., Miao, J., Li, G., Chen, T., Feng, L., and Zhang, J. 2024. “Performance Study of Ventilated Energy-Productive Walls: Experimental and Numerical Analysis.” *Solar Energy* 273: 112512.

[3] Xu, H., Yu, S., and Chen, Y. 2024. “Experimental and Theoretical Modelling of Fluctuating Internal Wind Pressures on a Ventilated Double Skin Facade of a Building.” *Energy and Buildings* 323: 114795.

[4] Watanabe, K., and Uematsu, Y. 2019. “Evaluation of Wind Loads on Ventilated Exterior Wall Systems.” *Journal of Wind Engineering JAWE 44* (2): 23-32. (in Japanese)

[5] American Society of Civil Engineers. 2012. “Wind Tunnel Testing for Buildings and Other Structures.” ASCE/SEI 49-12, Reston, VA, USA.

[6] Irwin, H. P., Cooper, K. R., and Girard, R. 1979. “Correction of Distortion Effects Caused by Tubing Systems in Measurements of fluctuating Pressures.” *Journal of Wind Engineering and Industrial Aerodynamics* 5: 93-107.

[7] Okuda, Y., and Taniike, Y. 1993. “Conical Vortices over Side Face of a Three-Dimensional Square Prism.” *Journal of Wind Engineering and Industrial Aerodynamics* 50: 163-72.

[8] Oh, J. H., Kopp, G. A., and Inculet, D. R. 2007. “The UWO Contribution to the NIST Aerodynamic Database for Wind Loads on Low Buildings: Part 3. Internal Pressures.” *Journal of Wind Engineering and Industrial Aerodynamics* 93: 31-59.

[9] Uematsu, Y., Yambe, T., and Yamamoto, A. 2022. “Application of a Numerical Simulation to the Estimation of Wind Loads on Photovoltaic Panels Installed Parallel to Hip Roofs of Residential Houses.” *Wind* 2: 129-49.

[10] Uematsu, Y., Yambe, T., and Yamamoto, A. 2022. “Wind Loading of Photovoltaic Panels Installed on Hip Roofs of Rectangular and L-Shaped Low-Rise Buildings.” *Wind* 2: 288-304.

[11] Gavanski, E., Takahashi, M., Uematsu, Y., and Morrison, M. 2015. “Quantitative Performance Evaluation of Time-Varying Wind Pressure Loading Actuator.” *AIJ Journal of Technology and Design* 21 (49): 1075-80. (in Japanese)

[12] Hosokawa, K. 2019. “Effects of Openings on the Wind Loads on Ventilated Exterior Wall Systems of Low-Rose Residential Houses.” Master’s thesis, Tohoku University. (in Japanese)